Lee, A.L., Flynn, P.F. & Wand, A.J. A comparison of 2H and 13C NMR relaxation techniques for the study of protein methyl group dynamics in solution. J. Am. Chem. Soc. 121, 2891–289…

3 AUTHORS, INCLUDING:

Andrew Joshua Wand
University of Pennsylvania
193 PUBLICATIONS **8,677** CITATIONS

Comparison of ²H and ¹³C NMR Relaxation Techniques for the Study of Protein Methyl Group Dynamics in Solution

Andrew L. Lee, Peter F. Flynn, and A. Joshua Wand*

Contribution from the The Johnson Research Foundation and Department of Biochemistry and Biophysics, University of Pennsylvania, Philadelphia, Pennsylvania 19104-6059

Abstract: A comparison of ²H- and ¹³C-based NMR relaxation methods to characterize the dynamics of methyl groups in proteins is presented. Using human ubiquitin as a model system, the field dependence of carbon and deuterium relaxation parameters has been measured and used to probe the utility of various forms of the model-free formalism in revealing the underlying dynamics. We find that both approaches reveal the same overall dynamical features provided that suitable parametrization and model-free spectral densities are employed. It is found that the original and extended model-free formalisms yield different descriptions of the methyl group dynamics and that the extended version is more appropriate for the analysis of carbon relaxation. Because of the inherent differences in the types of information that ²H and ¹³C offer, deuterium methods appear to provide robust access to methyl symmetry axis order with the least amount of data, while carbon methods provide more robust access to model-free parameters defining the time scale of methyl rotation and methyl symmetry axis motion.

Introduction

The influence and role of internal dynamics on protein stability, structure and function continues to be the subject of debate and extensive study.[1−6] While our knowledge of the structural taxonomy of proteins appears to be nearing completeness, our understanding of the existence, character, and interconversion of states near the lowest free energy state of proteins remains largely incomplete and unexplored. Important issues rest on the characterization of the internal dynamics of protein structures, particularly that of buried side chains.[7−12] A wide variety of experimental and theoretical techniques have been employed to characterize the internal motions of biopolymers. The use of NMR spectroscopy has recently been aided by the robustness of recently developed resonance assignment techniques[13−15] and the development of a range of isotopic enrich-

ment strategies.[16−23] Over the past decade, solution NMR relaxation studies of proteins have generally focused on the dynamics of the main chain.[24−31] More recently, the maturation of a variety of multidimensional NMR sampling of heteronuclear relaxation has begun to allow facile access to the motion of protein side chains.[20,32,33]

Here we are interested in comparing the information derived from ¹³C- and ²H-based relaxation studies of the ps−ns

* Correspondence author. Telephone: (215)-573-7288. Fax: (215)-573-7290. E-mail: wand@mail.med.upenn.edu.

(1) Careri, G.; Fasella, P.; Gratton, E. *Crit. Rev. Biochem.* **1975**, *3*, 141−164.

(2) Karplus, M.; McCammon, J. A. *Crit. Rev. Biochem.* **1981**, *9*, 293−349.

(3) Debrunner, P. G.; Frauenfelder, H. *Annu. Rev. Phys. Chem.* **1982**, *33*, 283−299.

(4) Englander, S. W.; Kallenbach, N. R. *Q. Rev. Biophys.* **1984**, *16*, 521−655.

(5) Williams, R. J. P. *Eur. J. Biochem.* **1989**, *183*, 479−497.

(6) Palmer, A. G.; Williams, J.; McDermott, A. *J. Phys. Chem.* **1996**, *100*, 13293−13310.

(7) Karplus, M.; Ichiye, T.; Petitt, B. M. *Biophys. J.* **1987**, *52*, 1083−1085.

(8) Frauenfelder, H. et al. *J. Phys. Chem.* **1990**, *94*, 1024−1037.

(9) Frauenfelder, H.; Sligar, S. G.; Wolynes, P. G. *Science* **1992**, *254*, 1598−1603.

(10) Wand, A. J.; Urbauer, J. L.; McEvoy, R. P.; Bieber, R. J. *Biochemistry* **1996**, *35*, 6116−6125.

(11) Li, Z.; Raychaudhuri, S.; Wand, A. J. *Protein Sci.* **1996**, *5*, 2647−2650.

(12) Yang, D.; Kay, L. E. *J. Mol. Biol.* **1996**, *263*, 369−382.

(13) Wüthrich, K. *NMR of Proteins and Nucleic Acids*; John Wiley & Sons: New York, 1986.

(14) Cavanagh, J.; Fairbrother, W. J.; Palmer, A. G.; Skelton, N. J. *Protein NMR Spectroscopy*; Academic Press: San Diego, 1996.

(15) Pelton, J. G.; Wemmer, D. E. *Annu. Rev. Phys. Chem.* **1995**, *46*, 139−167.

(16) Neri, D.; Szyperski, T.; Otting, G.; Senn, H.; Wüthrich, K. *Biochemistry* **1989**, *28*, 7510−7516.

(17) McIntosh, L. P.; Dahlquist, F. W. *Q. Rev. Biophys.* **1990**, *23*, 1−38.

(18) LeMaster, D. M. *Q. Rev. Biophys.* **1990**, *23*, 133−174.

(19) Kushlan, D. M.; LeMaster, D. M. *J. Biomol. NMR* **1993**, *3*, 701−708.

(20) LeMaster, D. M.; Kushlan, D. M. *J. Am. Chem. Soc.* **1996**, *118*, 9255−9264.

(21) Metzler, W.; Wittekind, M.; Goldfarb, V.; Mueller, L.; Farmer, B. T *J. Am. Chem. Soc.* **1996**, *118*, 6800−6801.

(22) Rosen, M. K.; Gardner, K. H.; Willis, R. C.; Parris, W. E.; Pawson, T.; Kay, L. E. *J. Mol. Biol.* **1996**, *263*, 627−636.

(23) Gardner, K. H.; Kay, L. E. *J. Am. Chem. Soc.* **1997**, *119*, 7599−7600.

(24) Kay, L. E.; Torchia, D. A.; Bax, A. *Biochemistry* **1989**, *28*, 8972−8979.

(25) Dellwo, M. J.; Wand, A. J. *J. Am. Chem. Soc.* **1989**, *111*, 4571−4578.

(26) Clore, G. M.; Driscoll, P. C.; Wingfield, P. T.; Gronenborn, A. M. *Biochemistry* **1990**, *29*, 7387−7401.

(27) Schneider, D. M.; Dellwo, M. J.; Wand, A. J. *Biochemistry* **1992**, *31*, 3645−3652.

(28) Stone, M. J.; Fairbrother, W. J.; Palmer, A. G.; Reizer, J.; Saier, M. H.; Wright, P. E. *Biochemistry* **1992**, *31*, 4394−4406.

(29) Mandel, A. M.; Akke, M.; Palmer, A. G. *J. Mol. Biol.* **1995**, *246*, 144−163.

(30) Dayie, K. T.; Wagner, G. *J. Am. Chem. Soc.* **1997**, *119*, 7797−7806.

(31) Fischer, M. W. F.; Zeng, L.; Pang, Y.; Hu, W.; Majumdar, A.; Zuiderweg, E. R. P. *J. Am. Chem. Soc.* **1997**, *119*, 12629−12642.

(32) Wand, A. J.; Bieber, R. J.; Urbauer, J. L.; McEvoy, R. P.; Gan, Z. *J. Magn. Reson. Ser B* **1995**, *108*, 173−175.

(33) Muhandiram, D. R.; Yamazaki, T.; Sykes, B. D.; Kay, L. E *J. Am. Chem. Soc.* **1995**, *117*, 11536−11544.

dynamics of methyl-bearing amino acid side chains. The recent emergence of suitable labeling strategies[20,33,34] now allows for the preparation of optimal samples. Methyl groups are of particular interest since they occur with high frequency and are often found in the hydrophobic cores of proteins. To gain confidence in and understanding of both ^{2}H and ^{13}C relaxation approaches to methyl dynamics, we present here a comparison of the two techniques applied to the methyl groups in recombinant human ubiquitin. Although similar comparisons have been carried out in the past in the context of small molecules,[35-37] the indirectly detected ^{2}H and ^{13}C relaxation techniques for proteins have not been compared. Here, 31 methyl groups have been examined and provide high statistical confidence for the comparison. A relatively broadly based set of relaxation data is used to probe the utility of various forms of the so-called model-free formalism of Lipari and Szabo[38,39] in revealing the dynamics underlying relaxation. The present paper is restricted to autocorrelation relaxation and it is noted that cross-correlation relaxation[31,40,41] can provide additional detail to the motions under consideration. We find that ^{2}H- and ^{13}C-based relaxation methods reveal the same dynamical features provided that suitable parametrization and model-free spectral densities are employed. Our results indicate that the original and extended model-free formalisms yield different descriptions of the dynamics and that the extended version is in general more appropriate for describing side-chain methyl dynamics. Because of the inherent differences in the types of information that ^{2}H and ^{13}C offer, the sensitivity of models and time scales to these data types are discussed in the context of currently available field strengths.

Theory

^{2}H and ^{13}C Relaxation. NMR spin relaxation is coupled to molecular motion through the spectral density function, $J(\omega)$, which is the cosine Fourier transform of the autocorrelation function, C(t), of the C−H bond vector for ^{13}C relaxation or the principal axis of the electric field gradient tensor for ^{2}H relaxation,

$$J(\omega) = 2\int_0^\infty C(t)\cos(\omega t)\,dt \qquad (1)$$

where C(t) is the product of the overall tumbling correlation function and the internal correlation function.[42] The precise relationship between the relaxation parameters and the spectral density depends on the mechanism of relaxation. In the case of ^{2}H (spin > $^1/_2$), relaxation is dominated by the quadrupolar mechanism, which for an axially symmetric electric field gradient is given by[43]

(34) Lee, A. L.; Urbauer, J. L.; Wand, A. J. *J. Biomol. NMR* **1997**, *9*, 437−440.
(35) Spiess, H. W.; Schweitzer, D.; Haeberlen, U. *J. Magn. Reson.* **1973**, *9*, 444−460.
(36) Vold, R. R.; Kobrin, P. H.; Vold, R. L. *J. Chem. Phys.* **1978**, *69*, 3430−3431.
(37) Brown, M. F. *J. Chem. Phys.* **1984**, *80*, 2832−2836.
(38) Lipari, G.; Szabo, A. *J. Am. Chem. Soc.* **1982**, *104*, 4546−4559.
(39) Lipari, G.; Szabo, A. *J. Am. Chem. Soc.* **1982**, *104*, 4559−4570.
(40) Daragan, V. A.; Mayo, K. H. *Prog. NMR Spectrosc.* **1997**, *31*, 63−105.
(41) Yang, D.; Mittermaier, A.; Mok, Y. K.; Kay, L. E. *J. Mol. Biol.* **1998**, *276*, 939−954.
(42) Abragam, A. *Principles of nuclear magnetism*, 1st ed.; Oxford University Press: Oxford, 1961; Vol. 32.
(43) Wittebort, R. J.; Szabo, A. *J. Chem. Phys.* **1978**, *69*, 1722−1736.

$$1/T_1(D) = \tfrac{3}{16}(e^2\,qQ/\hbar)^2[J(\omega_D) + 4J(2\omega_D)] \qquad (2)$$

$$1/T_{1\rho}(D) = \tfrac{1}{32}(e^2\,qQ/\hbar)^2[9J(0) + 15J(\omega_D) + 6J(2\omega_D)] \quad (3)$$

in which e$^2qQ/h$ is the quadrupolar coupling constant, and the $J(\omega)$ terms correspond to the spectral density function evaluated at zero, single-quantum ^{2}H, and double-quantum ^{2}H frequencies. It is generally assumed that the principal axis of the electric field gradient tensor is collinear with the C−D bond vector. As discussed below, this assumption may not be completely accurate for methyl groups.[35]

Relaxation of ^{13}C magnetization under the conditions depicted in Figure 1, i.e., in the absence of cross-correlation effects, is governed by the sum of the C−H dipolar interaction and ^{13}C chemical shift anisotropy (CSA):[42]

$$\frac{1}{T_1} = N\left(\frac{\hbar^2\gamma_H^2\,\gamma_C^2}{4r_{CH}^6}\right)\left(\frac{\mu_o}{4\pi}\right)^2 [3J(\omega_C) + J(\omega_H - \omega_C) +$$

$$6J(\omega_H + \omega_C)] + \frac{\omega_C^2\Delta\sigma^2}{3}J(\omega_C) \quad (4)$$

$$NOE = 1 + \frac{\gamma_H}{\gamma_C}\left(\frac{\hbar^2\gamma_H^2\,\gamma_C^2}{4r_{CH}^6}\right)\left(\frac{\mu_o}{4\pi}\right)^2 [6J(\omega_H + \omega_C) -$$

$$J(\omega_H - \omega_C)]NT_1 \quad (5)$$

in which γ_i and ω_i are the gyromagetic ratio and Larmor frequency of spin i, $\Delta\sigma$ ($= \sigma_\| - \sigma_\perp$) is the breadth of an axially symmetric ^{13}C chemical shift anisotropy, r_{CH} is the C−H bond distance, μ_o is the permittivity of free space, and N is the number of hydrogens directly bonded to ^{13}C.

Model-Free Spectral Densities. It is evident from the above equations that the interpretation of relaxation data depends critically upon the form of the spectral density function. A particularly useful form of $J(\omega)$ proposed by Lipari and Szabo consists of two internal motional parameters (S^2, τ_e) in addition to a parameter which corresponds to overall molecular reorientation (τ_m).[38,39] This so-called "model-free" form is given by

$$J(\omega) = \frac{2}{5}\left[\frac{S^2\tau_m}{1 + \omega^2\tau_m^2} + \frac{(1 - S^2)\tau}{1 + \omega^2\tau^2}\right] \qquad (6)$$

in which $\tau^{-1} = \tau_m^{-1} + \tau_e^{-1}$. S^2 is the generalized order parameter, which can take on a value between 0 and 1, corresponding to complete isotropic disorder and fixed orientation, respectively, of the relevant vector in the molecular frame. The τ_e parameter is the effective correlation time for the internal motion. The model-free spectral density allows for a separation between the relatively slow (ns) overall reorientational motion and the relatively fast (ps−ns) internal motion(s). An extension of the original model-free $J(\omega)$ allows for further separation of two internal motions on two time scales:[38,44]

$$J(\omega) = \frac{2}{5}\left[\frac{S_f^2\,S_s^2\tau_m}{1 + \omega^2\tau_m^2} + \frac{(1 - S_f^2)\tau_1}{1 + \omega^2\tau_1^2} + \frac{S_f^2(1 - S_s^2)\tau_2}{1 + \omega^2\tau_2^2}\right] \quad (7)$$

in which $\tau_1^{-1} = \tau_m^{-1} + \tau_f^{-1}$ and $\tau_2^{-1} = \tau_m^{-1} + \tau_s^{-1}$. The "f" and "s" subscripts refer to the fast and slow internal motions, respectively. Here, the *internal* correlation function is composed of two single-exponential terms. In this extended model-free

(44) Clore, G. M.; Szabo, A.; Bax, A.; Kay, L. E.; Driscoll, P. C.; Gronenborn, A. M. *J. Am. Chem. Soc.* **1990**, *112*, 4989−4991.

a

b

Figure 1. Modified pulse sequences of Nicholson et al.[47] for the measurement of methyl ^{13}C T_1 (a) and {^1H}−^{13}C NOE (b) at 14.1 T for proteins in 90% H_2O, 10% D_2O solution. Narrow bars and wide bars correspond to 90° and 180° RF pulses, respectively. The value of θ is adjusted such that $2\pi J_{CH}\tau = 54.7°$.[48,50] The value of Δ is set to $^1/_4 J_{CH}$ for maximal sensitivity; no difference in T_1 values was observed if Δ was set to $^1/_8 J_{CH}$. Development of the NOE via nonselective saturation of ^1H resonances is accomplished with ~10 kHz 120° ^1H pulses separated by 5 ms, shown in parentheses. In scheme a, saturation of ^1H resonances is continued during the variable T_1 relaxation delay period. During the t_1 evolution periods, ^1H decoupling is accomplished with a 3−6 kHz WALTZ-16 decoupling scheme. The phase cycle for scheme a is $\phi 1 = y,-y$; $\phi 2 = 4(y),4(-y)$; $\phi 3 = x,x,-x,-x$; rec $= x,-x,-x,x,-x,x,x,-x$. Z-axis gradients for the T_1 experiment were applied as follows: $g1 = 6$ G/cm; $g2 = 5$ G/cm; $g3 = 16$ G/cm; $g4 = 5$ G/cm; all gradients were applied for 0.5 ms. In scheme b, one experiment is recorded with ^1H saturation (in parentheses) and another without. The WATERGATE[73] sequence is used for solvent suppression. The phase cycle for scheme b is $\phi 1 = y$; $\phi 2 = x,-x$; rec $= x,-x$. If a ^1H composite 180 pulse is used instead for ^1H decoupling during t_1 evolution (see text), the composite pulse is cycled $x,-x$, and $\phi 1 = y$; $\phi 2 = x,x,-x,-x$; rec $= x,x,-x,-x$. Z-axis gradients for the NOE experiment were applied as follows: $g1 = 8$ G/cm; $g2 = 8$ G/cm; $g3 = 20$ G/cm; all gradients were applied for 0.5 ms. In T_1 and NOE experiments quadrature in t_1 is accomplished using States-TPPI phase cycling of $\phi 2$ and $\phi 1$, respectively.

form, there are four internal parameters that must be determined. To reduce the dimensionality of this problem, S_f^2 is often fixed at 0.111, which arises from an assumed tetrahedral geometry of the methyl group.[38,39,45]

Lipari and Szabo pointed out that given T_1 and NOE relaxation data at one or two fields, the simple model-free parameters (eq 6) are most reliably obtained when the internal motion is in the extreme narrowing limit. However, when data exist at multiple fields, the model-free formalism can provide a useful description for internal motion that is outside of the extreme narrowing limit.[38] In the case of the extended model-free formalism, the "slow" internal motion(s) must *not* be in extreme narrowing if it is to be discriminated from the fast internal motion(s). If both internal motions are in extreme narrowing, the extended model-free formalism is not warranted.

Experimental Section

Samples. In a manner similar to that of a previous study,[10] human ubiquitin used for ^2H relaxation studies was prepared by overexpression in *Escherichia coli* grown on media containing 50% H_2O, 50% D_2O, and using $^{15}NH_4Cl$ and D-glucose (U-$^{13}C_6$,99%) as the sole nitrogen and carbon sources, respectively. Purification was carried out essentially as reported previously.[10] The obtained protein was uniformly labeled in ^{15}N and ^{13}C, with methyl groups randomly fractionally deuterated to ~30%. NMR sample solution conditions were 90% H_2O, 10% D_2O, 50 mM acetate-d_3, pH = 5.0. The final protein concentration was 1 mM in a volume of 300 μL, which was transferred into a Shigemi NMR tube (Shigemi, Inc.; Allison Park, PA).

Ubiquitin used for ^{13}C relaxation studies was produced by overexpression in *E. coli* grown on pyruvate-containing media as described previously.[10,34] Isolated ^{13}C methyl groups were introduced into Leu δ, Val γ, and Ile $\gamma 2$ positions. Ala β carbons labeled with ^{13}C had a directly bonded $^{12}C_\alpha$ in 80−90% of the ubiquitin molecules. NMR sample solution conditions were 90% H_2O, 10% D_2O, 50 mM acetate-d_3, pH = 5.0, and the protein concentration was 2.2 mM. A final volume of 650 μL was transferred into a standard NMR tube.

NMR Spectroscopy. NMR experiments at 11.7, 14.1, and 17.6 T were conducted on Varian Unity Inova spectrometers equipped with $^1H/^{15}N/^{13}C$ probeheads with Z-axis pulsed-field gradients. The ^{13}C T_1 NMR experiment at 9.4 T was recorded on a wide bore Bruker DMX spectrometer equipped with a $^1H/^{15}N/^{13}C/^{31}P$ probehead with Z-axis pulsed-field gradients (at NMRFAM at the University of Wisconsin, Madison). All relaxation experiments were carried out at 30 °C, at which the temperature was calibrated using a methanol standard.[46]

Measurements of relaxation rates of multiple spin coherence involving deuterium, namely $R(I_zC_z)$, $R(I_zC_zD_z)$, and $R(I_zC_zD_y)$ were made at field strengths corresponding to ^2H frequencies of 92.09 and 115.24 MHz, resulting in six data sets. The increased resolution experimental pulse sequences of Kay and co-workers were used.[33] At 92 MHz, the following relaxation delay times were used: 10.05*, 14.0, 18.6, 23.5*, 29.0, 35.0, 42.0, 50.0*, and 60.0 ms for I_zC_z; 0.60, 4.55, 9.15, 14.15*, 19.55, 25.55, 32.55, 40.55, and 50.55 ms for $I_zC_zD_z$; 0.4*, 1.5, 3.3*, 5.9, 9.2, 13.3, 15.5, 18.1, 23.7*, and 30.0 ms for $I_zC_zD_y$. Asterisks indicate duplicate measurements. Recycle delay times of 1.6, 1.8, and 2.1 s and 16, 48, and 32 transients/fid were used for I_zC_z, $I_zC_zD_z$, and $I_zC_zD_y$, respectively. All three data sets at 92 MHz were acquired with 82* × 512* points for the ^{13}C (t_1) and ^1H (t_2) dimensions, respectively. The ^{13}C spectral widths and carrier frequencies were set to 19.22 and 17.68 ppm, respectively. At 115 MHz, the following relaxation delay times were used: 11.20, 15.15, 19.75, 24.65, 30.15, 36.15, 43.15, 51.15, and 61.15 ms for I_zC_z; 0.60, 4.55, 9.15, 14.15, 19.55, 25.55, 32.55, 40.55, and 50.55 ms for $I_zC_zD_z$; 0.4*, 1.5, 3.3*, 5.9, 9.2, 13.3, 18.1, 23.7*, and 30.0 ms for $I_zC_zD_y$. Recycle delay times of 2.1, 2.1, and 2.3 s were used for I_zC_z, $I_zC_zD_z$, and $I_zC_zD_y$, respectively, and 16 transients/fid were collected for each experiment. At 115 MHz, data sets were acquired with 102* × 512* points for the ^{13}C (t_1) and ^1H (t_2) dimensions, respectively. The ^{13}C spectral widths and carrier frequencies were set to 19.07 and 17.87 ppm, respectively. Approximately 158 h of spectrometer time was used for all of the ^2H experiments.

For the ^{13}C T_1 and {^1H}−^{13}C NOE experiments, previously published pulse sequences[47] were slightly modified and are reproduced in Figure 1. It was found that spectral artifacts in the {^1H}−^{13}C NOE experiment arising from a sample impurity were significantly reduced if a composite 180° ^1H pulse for t_1 ^1H decoupling was used instead of WALTZ-16. However, for the T_1 experiment WALTZ-16 ^1H decoupling was used to ensure that dipolar cross-correlation effects were minimized.[48−50]

(45) Woessner, D. E. *J. Chem. Phys.* **1962**, *36*, 1−4.
(46) Raiford, D. S.; Fisk, C. L.; Becker, E. D. *Anal. Chem.* **1979**, *51*, 2050−2051.
(47) Nicholson, L. K.; Kay, L. E.; Baldisseri, D. M.; Arango, J.; Young, P. E.; Bax, A.; Torchia, D. A. *Biochemistry* **1992**, *31*, 5253−5263.
(48) Palmer, A. G.; Wright, P. E.; Rance, M. *Chem. Phys. Lett.* **1991**, *185*, 41−45.
(49) Kay, L. E.; Torchia, D. A. *J. Magn. Reson.* **1991**, *95*, 536−547.
(50) Kay, L. E.; Bull, T. E.; Nicholson, L. K.; Griesinger, C.; Schwalbe, H.; Bax, A.; Torchia, D. A. *J. Magn. Reson.* **1992**, *100*, 538−558.

A total of four ^{13}C T_1 data sets were collected at field strengths corresponding to ^{13}C frequencies of 100.61, 125.71, 150.84, and 188.78 MHz. At 100 MHz, 120*(t_1) × 512*(t_2) spectra were recorded with T_1 relaxation delay times of 12.3, 42.3*, 102.3, 177.3*, 277.3, 402.3, 542.3*, 712.3, 902.3, and 1152.3 ms, where asterisks indicate duplicate measurements. Enhancement from the NOE was developed for 1.8 s, and the total recycle delay was 2.3 s. At 125 MHz, 100*(t_1) × 512*(t_2) spectra were recorded with T_1 relaxation delay times of 137.6, 248.2*, 388.8, 559.6, 765.6*, and 1001.8 ms. Enhancement from the NOE was developed for 2.3 s, and the total recycle delay was 3.0 s. At 150 MHz, 110*(t_1) × 512*(t_2) spectra were recorded with T_1 relaxation delay times of 12.0*, 62.3, 137.6, 248.0*, 388.6, 559.4, 765.2*, and 1001.2 ms. Enhancement from the NOE was developed for 2.3 s, and the total recycle delay was 3.0 s. At 188 MHz, 120*(t_1) × 512(t_2) spectra were recorded with T_1 relaxation delay times of 167.6, 298.1*, 468.7, 674.5, 915.4*, and 1201.4 ms. Enhancement from the NOE was developed for 2.5 s, and the total recycle delay was 3.3 s. In all T_1 experiments, the spacing between ^{1}H 120° pulses during NOE buildups and relaxation delay periods was set to 5 ms, except for the 100 MHz data set for which the spacing was set to 4.2 ms. A total of three {^{1}H}–^{13}C NOE experiments were collected at 125, 150, and 188 MHz. At each field strength, a reference experiment with no ^{1}H saturation and an experiment with ^{1}H saturation for approximately 10T_1 (6, 7, and 7 s for the three fields, respectively) were acquired in an interleaved manner (see Figure 1). NOE spectral parameters were identical to the T_1 parameters. A ^{13}C spectral width of 15.1 ppm was used for all of the ^{13}C relaxation experiments. For all experiments 8 transients/fid were collected, except the 125 MHz NOE for which 16 transients/fid were collected. Approximately 100 hours of spectrometer time was needed for these ^{13}C T_1 and NOE experiments.

Data Analysis. All data sets were processed into 512 × 1024 matrices using Felix 95.0 software (Molecular Simulations Inc., San Diego). Cross-peak intensities were used to quantitate ^{2}H or ^{13}C magnetization, and the uncertainties in these intensities were estimated from duplicate measurements (except for the NOE experiments, see below). The Levenberg–Marquardt algorithm[51] was used for nonlinear 2-parameter curve fits for all ^{2}H and ^{13}C decay data. On the whole, χ^2 residuals were lower than the number of data points in a given decay, signaling "good fits". All relaxation parameters are reported in the Supporting Information. Standard errors in the relaxation rate constants were taken from the covariance matrix, and re-acquisition of T_1 data sets confirmed this error estimation procedure.

Values of ^{2}H T_1 and $T_{1\rho}$ were deconvoluted from relaxation rates of I_zC_z, $I_zC_zD_z$, and $I_zC_zD_y$ coherences in the following manner:[33]

$$\frac{1}{T_1} = R_1(D) = R(I_zC_zD_z) - R(I_zC_z) \quad (8)$$

$$\frac{1}{T_{1\rho}} = R_{1\rho}(D) = R(I_zC_zD_y) - R(I_zC_z) \quad (9)$$

Average standard errors for these pure ^{2}H relaxation rates were 6.1 and 5.8% for T_1 and $T_{1\rho}$ at 92 MHz, and 7.2 and 6.3% for T_1 and $T_{1\rho}$ at 115 MHz, respectively. Average standard errors in ^{13}C T_1 values were 1.0, 1.2, 0.6, and 0.7% for 100, 125, 150, and 188 MHz data sets, respectively. {^{1}H}–^{13}C NOEs were calculated from peak intensity ratios, I^{NOE}/I^{ref}, taken from the NOE (^{1}H saturation) and reference (no ^{1}H saturation) experiments. Intensity uncertainties were estimated based on the root-mean-square noise level in the baseplane. To be conservative, this value was doubled and then propagated to yield NOE standard errors of 1–2% for all data sets. This practice was found to be realistic on the basis of a duplicate 150 MHz NOE experiment carried out several months later.

Internal dynamics parameters were fitted locally for each methyl site using a nonlinear least-squares Powell minimization[51] of the error function,

(51) Press: W. H.; Teukolsky, S. A.; Vetterling, W. T.; Flannery, B. P. *Numerical recipes in fortran 77: the art of scientific computing*, 2nd ed.; Cambridge University Press: Cambridge, 1992; Vol. 1.

$$\chi^2 = \sum_j^M \left(\frac{\text{obs}_j - \text{calc}_j}{\lambda_j^{\text{obs}}} \right)^2 \quad (10)$$

in which M is the number of relaxation measurements for a given spin, obs_j is the jth measured relaxation parameter, calc_j is the jth calculated relaxation parameter (from eqs 2–7), and λ_j^{obs} is the estimated uncertainty in obs_j. In the case of ^{2}H relaxation, e^2qQ/h was taken to be 165 kHz.[52] In the case of ^{13}C relaxation, $\Delta\sigma$ was fixed at 25 ppm,[53] and the effective C–H bond distance was taken to be 1.115 Å[54] (see Discussion). Variation of the breadth of the CSA tensor by ±25 ppm results in a change of less than 1% in obtained relaxation parameters. Because the Powell procedure does not in general locate global minima, it was necessary to perform an initial grid search of the relevant parameter space prior to the Powell minimization. Parameter errors were estimated from 150 Monte Carlo simulations.

Results

Methyl Dynamics Determined from ^{2}H Relaxation. The ^{2}H experiments and analysis were carried out as prescribed[33] (see Experimental Section). Relaxation rates of I_zC_z, $I_zC_zD_z$, and $I_zC_zD_y$ coherences were measured for ^{13}CH$_2$D isotopomers from 44 methyl groups in ubiquitin at 14.1 and 17.6 T at 30 °C. These rates were deconvoluted into pure ^{2}H longitudinal and transverse rates using eqs 8 and 9. Employing the model-free approach, S^2 and τ_e dynamics parameters were obtained via fits to eqs 2, 3, and 6. S^2_{axis} was obtained from $S^2_{\text{axis}} = S^2/0.111$, in which the factor 0.111 is derived from rapid rotation of a methyl group with tetrahedral geometry.[45] An overall rotational correlation time, τ_m, of 3.5 ns was used, which was estimated from ^{15}N T_1 and NOE data.[55] The best-fit model-free parameters are given in Table 1. On average, the experimental data were reproduced from the best-fit model parameters to within 2.3 (T_1) and 3.8% ($T_{1\rho}$).[56] Values of S^2_{axis} obtained from fits using the extended model-free formalism (eq 7) yielded essentially identical order parameters for most methyls, as pointed out previously.[33] However, τ_{axis} and τ_f parameters could not be fitted reliably. All ^{2}H-derived dynamics parameters mentioned from this point on will refer to those obtained using the simple model-free formalism (eq 6).

Methyl Dynamics Determined from ^{13}C Relaxation. Carbon T_1 and NOE relaxation measurements for 31 methyl groups in ubiquitin were recorded at 11.7, 14.1, and 17.6 T, and an additional T_1 data set was recorded at 9.4 T. Only 31 methyls could be characterized since the ^{13}C approach used does not label Thr γ and Ile δ methyl groups appropriately.[34] Within experimental error, no evidence for deviation from monoexponential decay was found in any of the T_1 data (Figure 2); excellent fits were obtained, resulting in T_1 uncertainties of 1% or less (Supporting Information). Therefore, the measured T_1's approximate the initial decay rates to better than 1%, strongly suggesting that dipole–dipole cross-correlation[57] may be ignored in this analysis. As pointed out previously, multiexponential behavior should become more severe as the correlation time corresponding to methyl 120° jumps decreases below 15 ps.[49]

(52) Mantsch, H. H.; Saito, H.; Smith, I. C. P. *Prog. Nucl. Magn. Reson. Spectrosc.* **1977**, *11*, 211–271.

(53) Spiess, H. W. *NMR: Basic Principles and Progress* **1978**, *15*, 55–214.

(54) Henry, E. R.; Szabo, A. *J. Chem. Phys.* **1985**, *82*, 4753–4761.

(55) Lee, A. L.; Wand, A. J. *J. Biomol. NMR* **1999**, *13*, 101–112.

(56) In the laboratory of Professor Lewis Kay, an independent study of ^{2}H methyl dynamics using a different ubiquitin sample was carried out using 11.7 and 14.1 T field strengths. Comparison of derived S^2_{axis} parameters from the two studies yielded excellent agreement within experimental error, with a pairwise rms deviation of 0.05.

(57) Werbelow, L. G.; Grant, D. M. *Adv. Magn. Reson.* **1977**, *9*, 189–299.

Table 1. Ubiquitin Methyl Simple Model-Free (SMF) Parameters from ^{2}H Relaxation at 30 °C

	S^2_{axis}	τ_e (ps)	χ^2_{M-n}		S^2_{axis}	τ_e (ps)	χ^2_{M-n}
I3$^\gamma$	0.98 ± 0.05	34.4 ± 3.1	0.3	I30$^\delta$	0.77 ± 0.05	12.5 ± 2.6	0.7
I3$^\delta$	0.75 ± 0.04	10.8 ± 2.2	0.6	I36$^\gamma$	0.83 ± 0.07	73.8 ± 4.2	0.4
V5$^{\gamma1}$	0.91 ± 0.05	35.7 ± 3.1	0.0	I36$^\delta$	0.58 ± 0.03	20.0 ± 1.6	0.6
V5$^{\gamma2}$	0.88 ± 0.04	19.2 ± 2.4	0.2	L43$^{\delta1}$	0.55 ± 0.11	57.3 ± 8.3	0.8
T7$^\gamma$	0.75 ± 0.04	42.8 ± 2.8	0.7	L43$^{\delta2}$	0.61 ± 0.05	31.9 ± 3.0	2.0
L8$^{\delta1}$	0.27 ± 0.02	43.1 ± 1.5	3.7	I44$^\gamma$	0.71 ± 0.05	40.2 ± 3.2	0.9
L8$^{\delta2}$	0.21 ± 0.02	42.5 ± 1.4	0.8	I44$^\delta$	0.31 ± 0.03	23.7 ± 1.7	5.9
T9$^\gamma$	0.64 ± 0.03	31.6 ± 1.8	3.8	A46$^\beta$	0.95 ± 0.04	16.4 ± 2.2	1.4
T12$^\gamma$	0.93 ± 0.05	33.5 ± 3.0	1.0	L50$^{\delta1}$	0.89 ± 0.12	21.5 ± 7.0	0.2
I13$^\gamma$	0.56 ± 0.03	38.7 ± 1.9	1.7	L50$^{\delta2}$	0.86 ± 0.09	17.7 ± 5.6	0.3
I13$^\delta$	0.55 ± 0.03	21.0 ± 1.8	0.2	T55$^\gamma$	0.93 ± 0.05	35.8 ± 3.0	1.0
T14$^\gamma$	0.78 ± 0.04	43.1 ± 2.8	0.3	L56$^{\delta1}$	0.60 ± 0.12	60.3 ± 8.1	0.0
L15$^{\delta1}$	0.58 ± 0.08	33.1 ± 5.5	0.2	L56$^{\delta2}$	0.62 ± 0.06	21.7 ± 4.2	0.0
L15$^{\delta2}$	0.62 ± 0.05	27.3 ± 3.0	1.3	I61$^\gamma$	0.95 ± 0.05	18.4 ± 2.6	0.5
V17$^{\gamma1}$	0.89 ± 0.06	39.3 ± 3.4	0.8	I61$^\delta$	0.56 ± 0.03	18.7 ± 2.0	0.9
V17$^{\gamma2}$	0.89 ± 0.09	72.1 ± 5.7	0.2	L67$^{\delta1}$	0.30 ± 0.03	51.4 ± 2.0	0.3
T22$^\gamma$	0.95 ± 0.05	28.4 ± 2.7	1.4	L67$^{\delta2}$	0.29 ± 0.03	42.6 ± 2.2	0.0
I23$^\gamma$	0.95 ± 0.05	24.5 ± 2.9	1.2	L69$^{\delta2}$	0.55 ± 0.05	37.0 ± 3.5	0.8
I23$^\delta$	0.51 ± 0.04	27.3 ± 2.3	0.2	V70$^{\gamma2}$	0.35 ± 0.04	73.1 ± 3.3	0.5
V26$^{\gamma1}$	0.86 ± 0.05	37.9 ± 3.1	1.5	L71$^{\delta1}$	0.29 ± 0.02	45.6 ± 1.6	1.1
V26$^{\gamma2}$	0.99 ± 0.05	10.3 ± 2.7	0.4	L73$^{\delta1}$	0.19 ± 0.01	40.0 ± 1.1	9.6
I30$^\gamma$	0.93 ± 0.05	24.6 ± 2.7	0.0	L73$^{\delta2}$	0.17 ± 0.01	35.7 ± 1.1	0.0
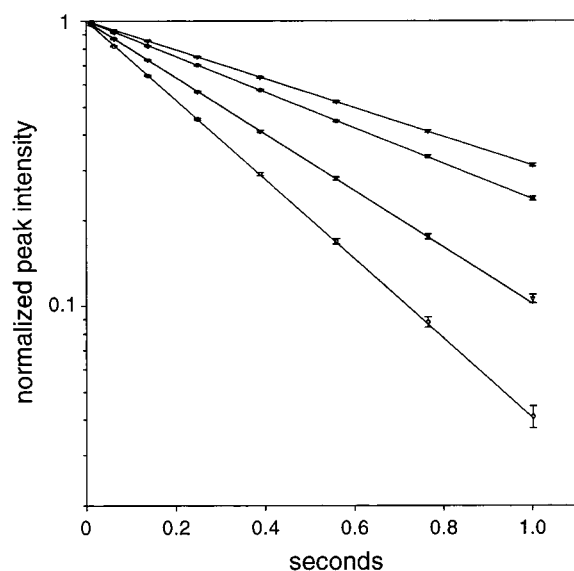
Figure 2. Time decays of ^{13}C longitudinal magnetization at 14.1 T (150 MHz ^{13}C frequency) plotted semilogarithmically. From top to bottom, normalized peak intensities for L50$^{\delta2}$, V5$^{\gamma2}$, V17$^{\gamma1}$, and I36$^\gamma$ methyl resonances are superimposed on their respective best-fitted single-exponential curves. The T_1 values, respectively, are 0.859, 0.697, 0.439, and 0.313 s.

Because methyl T_1's are dominated by this fast rotation and T_1's increase as τ_f decreases, protection against cross-correlation effects is automatically built into the T_1 experiment; methyls with longer T_1 values will be sampled in a manner which emphasizes the initial decay region, reducing the influence of cross-correlation to a negligible level.[47,49] The carbon T_1 and NOE data were initially analyzed using the original model-free parameters S^2_{axis} and τ_e (as in the ^{2}H analysis), fitting these parameters to eqs 4−6. Best-fit values of S^2_{axis} and τ_e are given in Table 2.

In addition, the relaxation data were also analyzed in model-free fashion allowing for two internal motion time scales with the parameters S^2_f, τ_f, S^2_s, and τ_s,[38,44,47] as shown in eq 7. This parameter set will be referred to as the extended model-free (EMF) description, whereas S^2_{axis} and τ_e corresponding to eq 6 will be referred to as the simple model-free (SMF) description,

following the convention introduced previously.[58] In the EMF formalism, the f (i.e. "fast") subscript corresponds to methyl rotation about the symmetry axis which generally occurs on a time scale faster than 100 ps. In our analysis using this two-time scale model, S^2_f is linked to τ_f and is fixed at 0.111, corresponding to perfect tetrahedral geometry of the methyl group. The s (i.e., "slow") subscript can correspond to reorientation of the methyl symmetry axis, which usually occurs on a time scale slower than methyl rotation. If both motions are on the same time scale, the EMF equations reduce to the SMF equations, and S^2_s becomes equivalent to $S^2/0.111$ of the SMF formalism. It should be noted that because S^2_f is fixed at 0.111, the EMF formalism may be inappropriate if the symmetry axis motion occurs on a time scale significantly faster than methyl rotation. For ubiquitin, this appears not to be a problem. We refer to the slow EMF parameters as τ_{axis} and S^2_{axis} for the remainder of this paper. Best-fit values of EMF parameters S^2_{axis}, τ_{axis}, and τ_f obtained from carbon T_1 and NOE data are given in Table 2. On average, the experimental data were reproduced from the best-fit model parameters to within 0.7 (T_1) and 1.2% (NOE). It should be mentioned that the 3-parameter EMF fits were more demanding than the 2-parameter SMF fits, resulting in larger standard errors in S^2_{axis} values. Nevertheless, removal of the 150 MHz T_1 and NOE data as well as the 125 MHz T_1 data resulted in essentially identical EMF parameters with only slightly larger error bars, suggesting that a reduced data set with good field dispersion is sufficient for EMF parameter fitting.

Inspection of Table 2 shows unequivocally that use of SMF and EMF formalisms give dramatically different order parameters for the methyl symmetry axis. S^2_{axis}(SMF) values greatly exceed S^2_{axis}(EMF) values when τ_{axis} > 400 ps, and in four instances S^2_{axis}(SMF) values exceed the physical limit of 1, suggesting that the SMF description has failed. Conversely, S^2_{axis}(SMF) and S^2_{axis}(EMF) values are in best agreement when τ_{axis} < 100 ps, such as for V5$^{\gamma1}$, V26$^{\gamma2}$, and I30$^\gamma$. In these cases both motions are near (or in) the extreme narrowing limit, and a single-exponential approximation of the internal autocorrelation function (i.e., SMF) yields accurate order parameters.

In ubiquitin, three types of methyl groups are adequately represented using the ^{13}C relaxation approach: Leu δ, Ile γ and

(58) Schurr, J. M.; Babcock, H. P.; Fujimoto, B. S. *J. Magn. Reson.* **1994**, *105(B)*, 211−224.

Table 2.   Ubiquitin Methyl Model-Free Parameters from ^{13}C Relaxation at 30 °C

	simple model-free (SMF)			extended model-free (EMF)			
	S^2_{axis}	τ_e (ps)	χ^2_{M-n}	S^2_{axis}	τ_f (ps)	τ_{axis} (ps)	χ^2_{M-n}
I3$^\gamma$	0.92 ± 0.03	31.3 ± 0.3	2.5	0.71 ± 0.07	28.1 ± 0.7	368 ± 58	0.6
V5$^{\gamma 1}$	0.83 ± 0.02	30.2 ± 0.3	1.4	0.80 ± 0.05	28.9 ± 1.1	109 ± 70	1.7
V5$^{\gamma 2}$	0.80 ± 0.02	18.4 ± 0.2	6.1	0.60 ± 0.05	14.1 ± 0.5	248 ± 21	1.6
L8$^{\delta 1}$	0.63 ± 0.02	30.6 ± 0.2	23.8	0.21 ± 0.04	22.0 ± 0.5	284 ± 12	4.9
L8$^{\delta 2}$	0.63 ± 0.02	27.7 ± 0.2	30.4	0.19 ± 0.04	18.9 ± 0.4	283 ± 10	2.6
I13$^\gamma$	1.00 ± 0.02	21.5 ± 0.2	23.8	0.52 ± 0.05	16.9 ± 0.4	477 ± 22	0.3
L15$^{\delta 1}$	0.76 ± 0.02	29.0 ± 0.2	16.2	0.40 ± 0.06	22.4 ± 0.6	309 ± 19	9.0
L15$^{\delta 2}$	0.62 ± 0.01	21.9 ± 0.2	11.0	0.39 ± 0.04	15.4 ± 0.5	214 ± 15	3.1
V17$^{\gamma 1}$	0.90 ± 0.03	34.9 ± 0.3	1.8	0.71 ± 0.07	31.7 ± 0.7	324 ± 48	0.2
V17$^{\gamma 2}$	1.16 ± 0.05	55.6 ± 0.6	1.4	**	53.9 ± 1.2	**	1.7
I23$^\gamma$	0.80 ± 0.02	23.7 ± 0.2	1.5	0.69 ± 0.07	20.9 ± 1.7	181 ± 92	0.5
V26$^{\gamma 1}$	0.94 ± 0.03	29.8 ± 0.3	4.7	0.67 ± 0.06	26.4 ± 0.6	406 ± 40	0.7
V26$^{\gamma 2}$	0.78 ± 0.02	15.5 ± 0.2	1.9	0.76 ± 0.03	15.0 ± 1.4	43 ± 62	2.4
I30$^\gamma$	0.84 ± 0.02	22.9 ± 0.2	2.8	0.81 ± 0.05	21.7 ± 1.2	108 ± 80	3.4
I36$^\gamma$	1.19 ± 0.05	52.0 ± 0.5	5.2	0.52 ± 0.08	47.3 ± 1.0	1460 ± 482	1.0
L43$^{\delta 1}$	0.89 ± 0.04	39.4 ± 0.4	6.5	0.50 ± 0.08	34.1 ± 0.8	399 ± 32	0.7
L43$^{\delta 2}$	0.75 ± 0.02	22.7 ± 0.2	22.0	0.35 ± 0.04	15.7 ± 0.4	303 ± 12	1.9
I44$^\gamma$	1.07 ± 0.03	28.6 ± 0.3	12.3	0.56 ± 0.07	24.3 ± 0.6	653 ± 75	0.8
A46$^\beta$	0.76 ± 0.02	18.0 ± 0.2	5.3	0.58 ± 0.05	13.6 ± 0.5	219 ± 23	2.1
L50$^{\delta 1}$	0.86 ± 0.02	23.3 ± 0.2	7.4	0.56 ± 0.05	18.6 ± 0.5	327 ± 23	0.9
L50$^{\delta 2}$	0.71 ± 0.01	13.7 ± 0.2	6.3	0.55 ± 0.04	8.8 ± 0.4	199 ± 18	1.3
L56$^{\delta 1}$	0.95 ± 0.04	44.5 ± 0.4	4.5	0.60 ± 0.10	40.1 ± 1.1	452 ± 84	1.0
L56$^{\delta 2}$	0.62 ± 0.01	18.7 ± 0.2	5.2	0.49 ± 0.05	13.5 ± 1.0	170 ± 29	2.8
I61$^\gamma$	0.81 ± 0.02	18.8 ± 0.2	4.1	0.71 ± 0.06	15.9 ± 1.3	179 ± 72	4.2
L67$^{\delta 1}$	0.63 ± 0.02	37.7 ± 0.3	11.9	0.25 ± 0.06	29.6 ± 0.6	282 ± 16	1.2
L67$^{\delta 2}$	0.60 ± 0.02	31.7 ± 0.3	13.8	0.25 ± 0.05	23.5 ± 0.6	261 ± 15	3.9
L69$^{\delta 2}$	0.81 ± 0.02	27.8 ± 0.2	6.1	0.54 ± 0.06	22.8 ± 0.6	296 ± 24	1.6
V70$^{\gamma 2}$	1.07 ± 0.04	47.9 ± 0.4	12.3	0.42 ± 0.09	41.6 ± 1.0	679 ± 89	3.3
L71$^{\delta 1}$	0.57 ± 0.02	33.0 ± 0.2	14.0	0.24 ± 0.05	24.9 ± 0.5	250 ± 14	2.8
L73$^{\delta 1}$	0.53 ± 0.01	27.1 ± 0.2	40.8	0.10 ± 0.03	17.3 ± 0.4	264 ± 8	7.7
L73$^{\delta 2}$	0.49 ± 0.01	23.7 ± 0.1	69.8	0.00 ± 0.03	12.5 ± 0.3	271 ± 6	3.3

Val γ methyl groups. Whereas Ile γ and Val γ had similar average S^2_{axis} values around 0.65, Leu δ methyls had a lower average S^2_{axis} value of 0.35, indicating a greater dynamical displacement from the main chain. The average τ_{axis} parameter was approximately 300 ps for Leu δ and Val γ but approached 500 ps for Ile γ methyls. In addition, the variability in τ_{axis} parameters differed significantly for the three methyl types. Standard deviations in τ_{axis} were 70, 470, and 230 ps for Leu δ, Ile γ, and Val γ methyls, respectively. No distinguishing characteristic values for the τ_f parameter were observed.

Comparison of ^2H and ^{13}C Dynamics Parameters. The comparison of ^{13}C-derived $S^2_{axis}(^{13}C,SMF)$ and $\tau_e(^{13}C)$ parameters with SMF parameters obtained from ^2H relaxation is shown in Figures 3a and 4a. Ideally, all points would fall along the diagonal if the two sets of parameters are in quantitative agreement. Obviously this is not the case since the correlation between S^2_{axis} parameters is weak at best. On the other hand, there is a strong correlation between τ_e parameters (Figure 4a), although the slope of the correlation is much greater than initially expected. At this point, it should be mentioned that using this simple form for $J(\omega)$, τ_e must be characteristic of both the motion *about* the methyl symmetry axis as well as motion *of* the symmetry axis. It follows that τ_e is a weighted average of the characteristic times of these two principal dynamic processes. Due to the geometry of the methyl group, the methyl rotation tends to dominate this average for all methyls in ubiquitin, and τ_e provides a reasonable estimate of τ_f for methyl rotation, as seen in Figure 4b. It is important to note that this property should not be a general one. In the case of ubiquitin, Figure 4a might initially suggest that CH_2D methyl rotation in the fractionally deuterated protein is ∼1.5 times slower than CH_3 rotation in the nondeuterated protein. However, it is likely that such an isotope effect, which was observed for methyl rotation in toluene,[35] is much smaller; numerical simulations to be presented

shortly which do not account for mass differences show that τ_e values determined from ^{13}C are expected to be approximately 10−40% shorter than τ_e determined from ^2H measurements. In any case, it is clear from these data that all of the methyl groups examined have model-free rotational correlation times shorter than 100 ps and that ^2H and ^{13}C relaxation SMF analyses yield τ_e values which are highly correlated.

Figure 3b shows the comparison of $S^2_{axis}(^2H)$ parameters with $S^2_{axis}(^{13}C,EMF)$ parameters. The $S^2_{axis}(^2H)$ values have a much stronger linear correlation with $S^2_{axis}(^{13}C,EMF)$ than with $S^2_{axis}(^{13}C,SMF)$. In addition, the average χ^2_{M-n} (χ-squared per degree of freedom) is reduced to 2.4 in the ^{13}C-EMF fits from an average value of 12.2 in the ^{13}C-SMF fits (Table 2). These results are not so surprising since there is no a priori reason methyl rotation and symmetry axis reorientation (via χ_1 and χ_2 rotations) should occur on the same time scale. *In conclusion, the extended model-free formalism, in which the internal autocorrelation function is composed of a sum of two single-exponentials, appears to be the simplest realistic description of side-chain methyl dynamics in ubiquitin.*

To further clarify the experimental comparisons in Figures 3 and 4, synthetic ^2H and ^{13}C relaxation parameters were generated for an ensemble of 100 methyl groups using the extended model-free formalism. Each methyl of the ensemble was randomly assigned S^2_{axis}, τ_{axis}, and τ_f values within the ranges of 0.05−0.90, 200−1000 ps, and 5−50 ps, respectively, and all methyls were arbitrarily defined by a τ_m of 4.0 ns and S_f^2 of 0.111. Deuterium T_1 and $T_{1\rho}$ at 92 and 115 MHz fields were generated for each methyl and subsequently fitted with SMF parameters. From the same ensemble, carbon T_1 and NOE data were generated for 100, 125, and 188 MHz and fitted with SMF and EMF parameters. These data, we believe, provide a reasonable model for the actual experimental data set and should thus facilitate interpretation. Figure 5a shows best-fit $S^2_{axis}(^2H)$ plotted
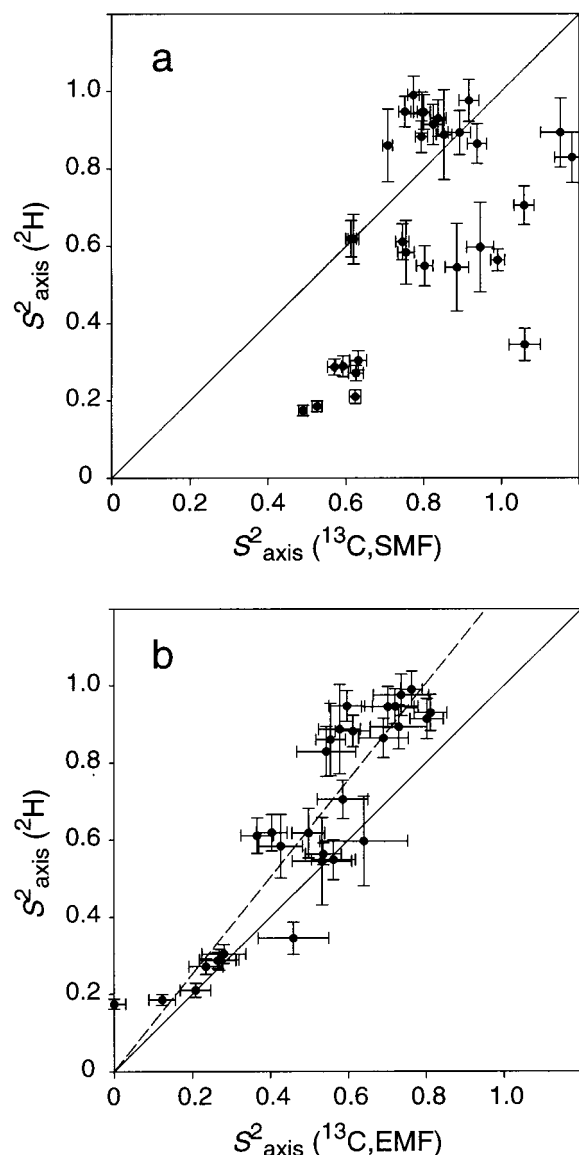
Figure 3. (a) Correlation of $S^2_{axis}(^2H)$ versus $S^2_{axis}(^{13}C,SMF)$. (b) Correlation of $S^2_{axis}(^2H)$ versus $S^2_{axis}(^{13}C,EMF)$. ^2H T_1 and $T_{1\rho}$ data were collected at 14.1 and 17.6 T, respectively. ^{13}C T_1 and NOE data were collected at 11.7, 14.6, 17.6 T, and an additional T_1 data set was collected at 9.4 T. Error bars correspond to standard deviations derived from 150 Monte Carlo simulations. The dashed line is a best-fit regression to the data forced through the origin, with a slope of 1.25 and a correlation coefficient of 0.83. In both (a) and (b), the value used for the overall correlation time, τ_m, was set to 3.5 ns. For the ^2H analysis, e^2qQ/h was set to 165 kHz, and for the ^{13}C analyses, r_{CH} was set to 1.115 Å.

versus best-fit $S^2_{axis}(^{13}C,EMF)$. Since the $S^2_{axis}(^{13}C,EMF)$ values were perfectly fitted to the correct values (as they must be when τ_m and S_f^2 are held fixed at their known values), it is clear that the SMF approximation for the ^2H analysis provides accurate order parameters except in the case of very low S^2_{axis} when τ_{axis} is large. In Figure 5b, the same $S^2_{axis}(^2H)$ parameters are plotted versus $S^2_{axis}(^{13}C,SMF)$ parameters, in a manner similar to that in Figure 3a. The shared feature of points falling below and to the right of the diagonal in these correlation plots illustrates just how devastating the SMF approximation can be for carbon T_1 and NOE relaxation data analysis (for the field strengths employed here) when the motion of the symmetry axis occurs on a significantly slower time scale than fast methyl rotation.
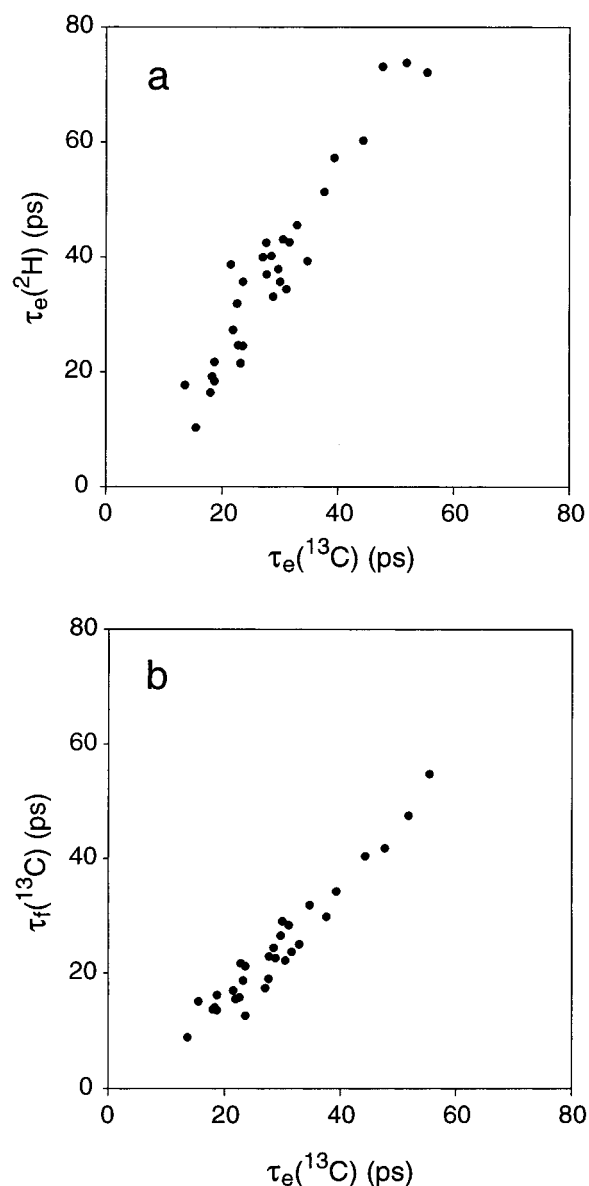
Figure 4. (a) Correlation of $\tau_e(^2H)$ versus $\tau_e(^{13}C)$. (b) Correlation of $\tau_e(^{13}C)$ versus $\tau_f(^{13}C)$. τ_e is the internal effective correlation time using the SMF formalism, and τ_f is the fast internal correlation time (corresponding to rotation about the methyl symmetry axis) using the EMF formalism. ^2H T_1 and $T_{1\rho}$ data were collected at 14.1 and 17.6 T. ^{13}C T_1 and NOE data were collected at 11.7, 14.6, 17.6 T, and an additional T_1 data set was collected at 9.4 T. Relevant fitting parameters are the same as in Figure 3.

Accordingly, we must now consider the S^2_{axis} values reported earlier by us to be quantitatively in error.[10] The similarity of Figures 3a and 5b is consistent with methyl dynamics being best described by the extended model-free formalism. In Figure 5c, $\tau_e(^2H)$ is plotted versus $\tau_e(^{13}C)$. From this plot it now becomes clear that the $\sim$1.5 slope in Figure 4a arises largely from different model dependencies of ^2H and ^{13}C relaxation data, complicating the matter of whether CH_3 and CH_2D groups undergo rotation at different rates. Given that nearly all methyls in ubiquitin have $\tau_{axis} < 600$ ps (corresponding to filled circles in Figure 5), the slope of the points in Figure 4a may be indicative of slightly slower methyl rotation rates for CH_2D groups in the deuterated protein relative to CH_3 groups in the nondeuterated protein.

These simulations do not reveal the origin of the observed slope of $\sim$1.25 in Figure 3b. The correlation between $S^2_{axis}(^2H)$
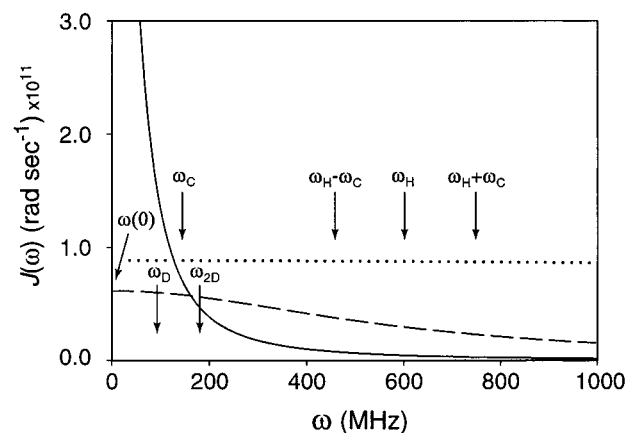
Figure 6. Simulated terms of the extended model-free (EMF) spectral density expression given by eq 7. The solid line represents the first term for overall rotation with a τ_m of 3.5 ns. The dotted line represents the second term for the fast motion, $\tau_f = 25$ ps. The dashed line represents the third term for slow or intermediate motion corresponding to reorientation of the methyl symmetry axis, $\tau_{axis} = 300$ ps. Labeled arrows correspond to the probing frequencies for ^{13}C and ^2H relaxation at 14.1 T (600 MHz ^1H frequency).

and $S^2_{axis}(^{13}C,EMF)$ values can be expressed as

$$S^2_{axis}(^2H) = \alpha S^2_{axis}(^{13}C,EMF) \tag{11}$$

The observed deviation of α from 1 can conceivably arise from a large number of contributions. In one class of potential sources, the deviation can arise from improperly set model-free parameters or constants assumed to be known, most of which will be considered in the Discussion. The value of τ_m used, for example, can be shown to empirically scale the value of α. A τ_m value of $\sim$4.1 ns will reduce α to 1, but this is an unreasonably large value of τ_m for 1–2 mM ubiquitin at 30 °C,[55] suggesting that the choice of τ_m is not the source of the discrepancy. The origin for the opposite dependencies of $S^2_{axis}(^2H)$ and $S^2_{axis}(^{13}C)$ upon τ_m lies in the inherently different frequency information in these relaxation data sets. To first order, $S^2_{axis}(^2H)$ and τ_m compensate for each other because the $J(0)$ term in the $T_{1\rho}$ expression (eq 3) must be satisfied by the $S^2 \tau_m /(1 + \omega^2 \tau_m 2)$ term in eq 6. On the other hand, for $\omega\tau_m > 1$, $S^2_{axis}(^{13}C)$ and τ_m must both increase in order to maintain ^{13}C spectral densities determined from T_1 and NOE data, which contain no $J(0)$ terms.

Discussion

The ^2H and ^{13}C relaxation parameters considered here provide complementary information with respect to methyl dynamics. This is largely due to the characteristic sampling frequencies which contribute to the various relaxation parameters (eqs 2–5). Specifically, ^2H favors the low frequencies because it samples at 0, 92, and 184 MHz at 14.1 T, for example, whereas ^{13}C favors higher frequencies, sampling at 150, 450, 600, and 750 MHz. This puts ^2H further into the extreme narrowing limit with respect to internal motion than ^{13}C, as shown in Figure 6. In addition, the presence of a $J(0)$ contribution to relaxation dramatically facilitates determination of S^2_{axis}. As a result, *^2H relaxation is an effective technique for obtaining S^2_{axis} regardless of time scales*[33] (at least in the range of 0 ps to near τ_m). The broader range of ^{13}C sampling frequencies results, as we shall soon see, in a greater sensitivity to two or more motions on different time scales up to approximately 1 ns, and it is often the case that two time scales can be discriminated and hence reliably fitted to EMF parameters. From Table 2 (and Figures

Figure 5. Simulation of ^2H and ^{13}C relaxation data using the extended model-free (EMF) form of $J(\omega)$ for an ensemble of 100 methyl groups with $\tau_m = 4.0$ ns and $S_f^2 = 0.111$. Each methyl was randomly assigned S^2_{axis}, τ_{axis}, and τ_f values in the ranges of 0.05–0.90, 200–1000 ps, and 5–50 ps, respectively. Fixing τ_m and S_f^2 at their correct values, these EMF-simulated data were subsequently fitted with SMF or EMF parameters (assuming the correct values of τ_m and S_f^2). ^2H T_1 and $T_{1\rho}$ were simulated at 11.7 and 14.1 T, and ^{13}C T_1 and NOE data were simulated at 9.4, 11.7, and 17.6 T. All data were given 1% error except for the $\{^1H\}-^{13}C$ NOE, which was given 2% error, to mimic realistic weighting for all fits (eq 10). (a) $S^2_{axis}(^2H)$ values are plotted versus the perfectly fitted, $S^2_{axis}(^{13}C,EMF)$ values. (b) $S^2_{axis}(^2H)$ values are plotted versus $S^2_{axis}(^{13}C,SMF)$ values. (c) $\tau_e(^2H)$ are plotted versus τ_e-(^{13}C). In all panels, methyl groups with true τ_{axis} values of 200–600 ps are represented by closed circles, whereas methyl groups with true τ_{axis} values of 600–1000 ps are represented by open circles.

3 and 4) it is clear that for ^{13}C data the SMF and EMF formalisms give quite different results and that the EMF formalism is preferred for describing ps–ns methyl dynamics. Interpretation of the carbon T_1 and NOE data using SMF parameters yields unreliable S^2_{axis} values which are often overestimated, as confirmed by simulations (Figure 5b). For the ^{2}H analysis, interpretation using EMF parameters was unsuccessful given the precision of the data.

Accessibility of Methyl Dynamics Parameters. Given that ^{2}H and ^{13}C have different sensitivities to different model-free parameters, it is of interest to define the limits of accessible time scales which can be characterized by ^{2}H and ^{13}C relaxation analyses. If the SMF formalism is used, it is desirable to be in the extreme narrowing limit, where reliable S^2_{axis} and τ_e values can be obtained with a minimum amount of data.[38] The lower frequencies of ^{2}H are preferable to ^{13}C in this regard. But because the SMF formalism is an oversimplification for methyl dynamics in proteins, ascribing significance to τ_e can become ambiguous, and little can confidently be said about motional time scales. If the EMF formalism is used, it is desirable for fitting purposes to have the fast motion in the extreme narrowing limit such that it acts as a simple scaling factor for T_1 and to have the slow motion such that $\omega\tau \approx 1$, as for ^{13}C relaxation in Figure 6. These ranges will be modulated by changing the field strength, and the correlation times will be better characterized if several fields are used so that the sampling frequencies span the putative Lorentzian line shape corresponding to τ_{axis} (i.e., τ_2 in eq 7).

These sensitivities are graphically demonstrated within the EMF formalism in the contour plots of Figure 7. In panel a, contour lines map calculated deuterium T_1 and $T_{1\rho}$ at 14.1 T as a function of τ_f and τ_{axis}, for a τ_m of 3.5 ns and S^2_{axis} of 0.5 (and S_f^2 of 0.111). The intersection of T_1 (solid) and $T_{1\rho}$ (dashed) contour lines define the τ_f/τ_{axis} values which give rise to those T_1 and $T_{1\rho}$ values. Conversely, values of τ_f and τ_{axis} which can be discriminated are characterized by an intersection of lines. Discrimination via ^{2}H relaxation of fast and slow time scales is optimal for 0.8 ns $\leq \tau_{axis} \leq$ 1.8 ns and 1 ps $\leq \tau_f \leq$ 60 ps. Outside of this region, curves for deuterium T_1 and $T_{1\rho}$ tend to run parallel within typical experimental error and thus it becomes a greater challenge to determine unique τ_f and τ_{axis} values. In panel b, similar contour lines are mapped for carbon T_1 (solid) and NOE (dashed) data at 14.1 T using identical EMF parameters. Here the region of optimal discrimination is roughly defined by 150 ps $\leq \tau_{axis} \leq$ 800 and 1 ps $\leq \tau_f \leq$ 50 ps. Due to the unique frequency dependence of the NOE, there is a higher propensity for intersection of T_1 and NOE lines than in panel a. When typical experimental errors are taken into account, ^{13}C relaxation is clearly the method of choice, given presently available field strengths, for discrimination of these motions when $\tau_{axis} <$ 1 ns. Analogous plots with τ_m set to 10 ns have intersection features indistinguishable from Figure 7. It is important to note that although these contour plots show representative features of dynamics time scales accessible from ^{2}H or ^{13}C relaxation, they do not account for variation in S^2_{axis} and field dependent effects.

The implications of these ^{2}H and ^{13}C contour plots have been confirmed by numerical simulations in which ^{2}H and ^{13}C data were synthesized with Gaussian noise using the EMF formalism and subsequently fitted with EMF parameters (data not shown). For typical deuterium T_1 and $T_{1\rho}$ experimental uncertainties (3–4%), field strengths in excess of 22 T (^{1}H frequency of 1000 MHz) in addition to lower field data (~11 T) were required to robustly fit τ_{axis} values in the range of 200–500 ps, into which
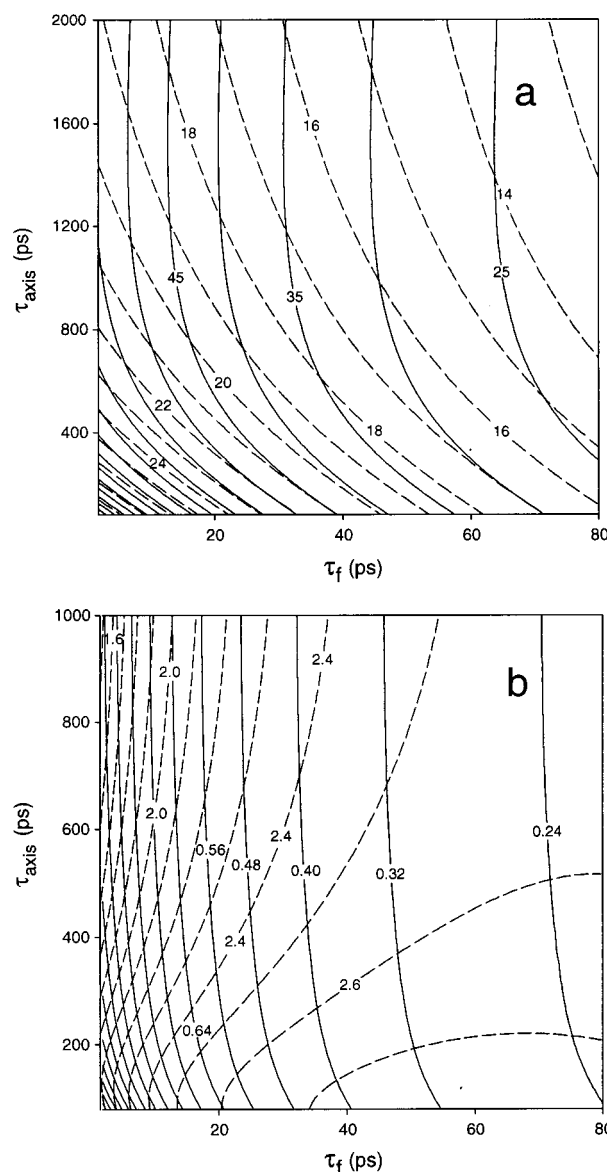

Figure 7. Contour plots of calculated ^{2}H (a) and ^{13}C (b) relaxation parameters at 14.1 T as a function of τ_f and τ_{axis} of the EMF formalism (eq 7). In (a), solid and dashed contour lines represent ^{2}H methyl (CH$_2$D) T_1 and $T_{1\rho}$ values, respectively. In (b), solid and dashed contour lines represent ^{13}C methyl (CH$_3$) T_1 and NOE values, respectively. For all cases, τ_m was fixed at 3.5 ns, S^2_{axis} was fixed at 0.5, and S_f^2 was fixed at 0.111. The intersection of solid and dashed lines indicate discrete solutions in τ_f/τ_{axis} space. Regions where solid and dashed lines are parallel indicate multiple solutions or ambiguity in defining τ_f and τ_{axis}.

many methyl τ_{axis} values in ubiquitin appear to fall (Table 2). This explains why attempts to fit τ_{axis} parameters (i.e., using the EMF formalism) to our experimental ^{2}H data failed in all cases.

A potential drawback for ^{13}C EMF analysis, at least with the present T_1 and NOE data, is that the lack of a $J(0)$ term in eqs 4 and 5 makes extraction of S^2_{axis} potentially challenging if the motion(s) of the symmetry axis is removed from the extreme narrowing limit. Careful inspection of simulations reveal that S^2_{axis} is fitted less robustly as τ_f increases, a feature that is also evident from the increased spacing of contour lines in Figure 7b as τ_f increases. This partially explains why S^2_{axis} and τ_{axis} for V17$^{\gamma 2}$ could not be fitted, since it had the highest τ_f value of ~54 ps.[59] If, in addition, τ_{axis} was greater than 1 ns, this

would further increase the difficulty of the fit since T_1 and NOE contour lines begin to run parallel in this regime (Figure 7b). If T_1 data at lower field strengths are recorded such that $(\omega_C\tau_{axis})^2 \ll 1$, S^2_{axis} will be obtained with increased precision as the putative Lorentzian spectral density line shape corresponding to the third term in eq 7 is mapped at lower frequency. Therefore, the available field strengths will represent an important constraint on the precision of the ^{13}C-derived S^2_{axis} estimates.

Simulations have confirmed that an optimal ^{13}C relaxation data set would consist of T_1 and NOE at a low field (e.g., 7 T or lower), a high field (e.g., 14.1 or 17.6 T), and if possible at an intermediate field. Due to the sensitivity of the experiments, the data should not require more than 100 h of acquisition time, and reasonably small uncertainties for S^2_{axis} and τ_{axis} values should be attainable. In principle, the accurate measurement of carbon T_2 would alleviate the challenge of determining S^2_{axis} with high precision when only high fields are available. However, accurate determination of methyl carbon transverse relaxation rates is especially difficult.[49]

Complex Motions. It is possible that even the extended model-free formalism (EMF) is an oversimplification of the dynamics in ubiquitin. For example, if, in addition to a 200 ps motion, there was an additional symmetry axis motion on a time scale of ~1 ns, the S^2_{axis}(^{13}C,EMF) would likely differ from S^2_{axis}(^{2}H). S^2_{axis}(^{2}H) would be an accurate order parameter for the combined slow motions (as long as $S^2_{axis} > 0.2$, see Figure 5a), whereas S^2_{axis}(^{13}C,EMF) could float from this value since it would not be anchored by a $J(0)$ or similar term. Therefore, points that fall off the line in Figure 3b may be indicative of motions more complex than the EMF formalism can accommodate. The methyl of L73$^{\delta2}$ may be a good candidate for such complex motions. This side chain is near the C-terminus, is highly solvent-exposed and is therefore likely to have more complex dynamics. Another may be V70$^{\gamma2}$, which falls below the diagonal in Figure 3b, and is also highly solvent-exposed.

Choices of "Fixed" Parameters—Effect on α. The observed discrepancy between S^2_{axis}(^{2}H) and S^2_{axis}(^{13}C,EMF) values, or deviation of the α parameter from 1 (eq 11), could arise from a number of sources, such as the chosen values of fixed parameters in the ^{2}H and ^{13}C analyses. The effect of τ_m was considered earlier, and now we discuss the remainder.

An issue brought up in recent ^{13}CH$_3$ relaxation studies is the geometry of the methyl group in various amino acids.[10,47,60] Specifically, the order parameter for methyl rotation depends on the angle β formed between the C—H (or C—D) bond and the symmetry axis:[38,39,45]

$$S_{Woessner} = \frac{3\cos^2\beta - 1}{2} \qquad (12)$$

Although the value of $S_{Woessner}$ ($= S_f = \sqrt{0.111}$) employed has a dramatic effect on S^2_{axis}, we have used the same value for ^{2}H and ^{13}C analyses and therefore this parameter does not effect the comparison. If, however, the *true* values of $S_{Woessner}$ differ for CH$_2$D and CH$_3$ groups, such differences would be manifested in α. It is interesting to note that values of S_f^2 less than 0.111 may be warranted (due to deviation from tetrahedral geometry[60–63]), which would increase the values of S^2_{axis} in Tables 1

and 2, and Figure 3. Because S^2_{axis}(^{2}H) values are already very close to 1, the adjusted S^2_{axis} values would then exceed 1 and cease to be physically meaningful. The S^2_{axis}(^{13}C,EMF) values, however, presently do not exceed 0.8, leaving room for such adjustments. If β is indeed greater than 109.5° for CH$_3$ and CH$_2$D, this may indicate that the methyl dynamics are more accurately characterized by the ^{13}C approach.

For ^{2}H relaxation, β is more accurately defined by the angle formed between the methyl symmetry axis and the principal axis of the electric field gradient tensor, which runs approximately collinear with the C—D bond vector. Thus, to interpret ^{2}H data accurately, the magnitude of e^2qQ/h in addition to the orientation of the field gradient needs to be known to high accuracy. If the field gradient axis and C—D bond vector orientations differ by as little as a few degrees (i.e., a change in β) as previously suggested,[35] S_f^2 could change by as much as 30%. Quadrupolar coupling constants of 165−168 kHz have been employed in this and previous methyl ^{2}H relaxation studies by Kay and co-workers.[33,64,65] Most studies in the solid state have also employed a narrow range of values for the CD$_3$ quadrupolar coupling constant, usually 160−170 kHz.[52] These values are vibrationally averaged (see next paragraph) since they are based directly on experimentally observed splittings.

For ^{13}C relaxation analysis, the C—H bond distance, r_{CH}, must be known to high accuracy in order to extract unbiased dynamics parameters. Because r_{CH} is taken to the sixth power, apparently small variations in r_{CH} can have correspondingly dramatic effects on calculated carbon T_1 values. Values of r_{CH} ranging from 1.07 to 1.14 Å have been implemented in the literature, resulting in a scaling factor which can vary by as much as 45%, a range much larger than any experimental T_1 uncertainties. Henry and Szabo[54] give a compelling recommendation for an effective methyl C—H bond length of 1.115 Å. This value effectively removes the contributions to relaxation from ultrafast stretching and reorientational librational motions of the C—H vector, which would otherwise be inappropriately reflected in S^2_{axis}.[54] For methine carbons, a value of 1.10 Å is recommended, which removes effects that arise from the bond stretching motions only, and hence the ultrafast reorientational motions of the vector are reflected in the order parameter.[54] With respect to the S^2_{axis} discrepancy in Figure 3b, an unreasonably large value of r_{CH} (>1.14 Å) must be employed to bring α to 1. It appears, unfortunately, that further investigation will be necessary to pinpoint the origin(s) of the nonunity value of α.

Potential Sources of Systematic Error. Of primary concern at the outset of this and previous ^{13}C-based autocorrelation studies was the effect of cross-correlations on ^{13}C relaxation.[57] Though ^{1}H−^{13}C dipolar cross-correlation is eliminated by ^{1}H decoupling/saturation, the degree of cross-correlation between protons within a methyl group,[49] although effectively small (Figure 2), remains unclear. In the ^{1}H-dense environment of proteins, it is assumed that the surrounding ^{1}H dipolar field is sufficient to efficiently mix the methyl group's manifold of spin states. From Figures 3b and 4b it appears that ^{2}H and ^{13}C dynamics are in good agreement and therefore suggests that cross-correlation is not an obstacle to meaningful interpretation of the ^{13}C data.

While neighboring ^{1}H spins provide favorable *indirect*

(59) Interestingly, this effect is the opposite of that observed for the ^{2}H-EMF fits, in which S^2_{axis} was fitted accurately but τ_f and τ_{axis} were not.

(60) Chatfield, D. C.; Szabo, A.; Brooks, B. R. *J. Am. Chem. Soc.* **1998**, *120*, 5301−5311.

(61) Lehmann, M. S.; Koetzle, T. F.; Hamilton, W. C. *J. Am. Chem. Soc.* **1972**, *94*, 2657−2660.

(62) Koetzle, T. F.; Golic, L.; Lehmann, M. S.; Verbist, J. J.; Hamilton, W. C. *J. Chem. Phys.* **1974**, *60*, 4690−4696.

(63) Batchelder, L. S.; Niu, C. H.; Torchia, D. A. *J. Am. Chem. Soc.* **1983**, *105*, 2228−2231.

(64) Kay, L. E.; Muhandiram, D. R.; Farrow, N. A.; Aubin, Y.; Forman-Kay, J. D. *Biochemistry* **1996**, *35*, 361−368.

(65) Yang, D.; Mok, Y. K.; Forman-Kay, J. D.; Farrow, N. A.; Kay, L. E. *J. Mol. Biol.* **1997**, *272*, 790−804.

interactions for suppression of cross-correlation effects, *direct* dipolar interactions with ^{13}C may contribute to the measured T_1 values. In a typical leucine side chain, for example, the $^1H^\gamma$ can in principle contribute to $^{13}C^\delta$ longitudinal or transverse relaxation on the order of a few percent, assuming a $^1H^\gamma - ^{13}C^\delta$ distance of 2.15 Å. If true, the ^{13}C-derived model-free parameters may be offset by a similar degree. It is interesting that this type of effect tends to *decrease* fitted $S^2_{axis}(^{13}C, EMF)$ values, at least for dynamics typical for Table 2, and hence cannot be invoked to explain the observed slope in Figure 3b. In contrast, neighboring spins are likely to have a negligible effect on the steady state $\{^1H\}$-^{13}C NOE (for nonselective ^1H saturation).[66]

For the ^2H approach, misinterpretation of $T_{1\rho}$ could be problematic if chemical exchange processes occur on microsecond time scales too rapid for the removal of these effects by the ~1 kHz spin-lock employed here.[67] Such effects, if present, would yield underestimated $T_{1\rho}$ values, which in turn yield overestimated S^2_{axis} parameters. Similarly for ^{13}C, an underdeveloped NOE would likely introduce error into S^2_{axis}, although this effect on S^2_{axis} is more difficult to predict.

Finally, one cannot ignore the possibility that deuteration of proteins has an effect on protein dynamics. For example, based upon Figures 4a and 5c, as well as previous observations,[35] the isotope effect on the rate of rotation about the symmetry axis cannot be completely dismissed. On the other hand, it is also possible that the methyl rotation rates in ubiquitin are too slow to be influenced by inertial effects.[68] As deuteration has been suggested to significantly perturb protein stability,[69-71] it is also plausible that many types of motions are affected by isotopic substitution. In conclusion, with all of the above-mentioned potential sources for scatter and bias in the respective analyses, the dynamical features of ubiquitin as revealed by ^2H and ^{13}C relaxation must be taken as remarkably similar.

Methyl Rotation. The model-free correlation time corresponding to rapid rotational methyl jumps (τ_f) is determined with extremely high precision from the ubiquitin ^{13}C relaxation data. In the case of ^2H relaxation, reasonable estimates for methyl rotation correlation times are obtained from the SMF formalism, as evidenced from the relatively tight correlation between $\tau_e(^2H)$ and $\tau_e(^{13}C)$ (Figure 4a) and between $\tau_e(^{13}C)$ and $\tau_f(^{13}C)$ parameters (Figure 4b), thus establishing confidence in these parameters. Even though some scatter exists between τ_e-(^2H) and $\tau_e(^{13}C)$, the simulations above show that this degree of scatter is expected when EMF data is fitted using the SMF formalism (Figure 5c). Therefore, aside from the slope, which indicates that CH$_2$D groups may rotate slightly more slowly than CH$_3$ groups, the correlation is essentially as good as one could expect. Accordingly, the EMF τ_f parameters in Table 2 are expected to be accurate model-free correlation times for rotation about the methyl symmetry axis, ranging from 8 to 54 ps with an average of 23.9 ± 10.6 ps.

The high precision with which τ_f and τ_e were obtained is in contrast to what is normally encountered in amide ^{15}N relaxation analyses, in which the τ_e parameter typically has a large relative uncertainty. Two reasons why τ_e (or τ_f) is fitted reliably for ^{13}C methyl relaxation are apparent: (1) the ^{13}C Larmor frequency is ~2.5 times greater than that for ^{15}N, resulting in greater sensitivity to fast motions in both T_1 and NOE data, (2) the very large amplitude of motion for methyl rotation is the dominant mechanism for scaling of T_1, as can be from eqs 4 and 7. In the case of ^2H relaxation, the latter reason alone is sufficient for robust fitting of τ_e.

Practical Considerations for ^2H and ^{13}C Relaxation Measurements and Analysis. To carry out the ^2H or ^{13}C experiments, the sample must have suitable isotopic incorporation. At current isotope prices the cost of making protein uniformly ^{13}C-enriched, 50% randomly fractionally ^2H-enriched protein is approximately 40% of the cost of making protein with isolated ^{13}C sites in methyl groups.[34] In addition, the ^2H strategy labels all methyl groups, whereas the ^{13}C strategy fails to label Met ϵ, Ile δ, and Thr γ methyls, although these methyls should be amenable to ^{13}C studies with old and new labeling schemes.[23,72] If the random fractional ^{13}C strategy is used,[32] the cost is negligible, and all methyl sites are enriched at a 15-20% level.

The sensitivities of the ^{13}C relaxation experiments, in our hands, are nearly an order of magnitude more sensitive than the ^2H relaxation experiments. In the present case, considering the different sample concentrations, roughly the same amount of spectrometer time was used for ^2H and ^{13}C approaches. Even though the precision of the extracted ^2H relaxation rates were 5-10 times lower than those of ^{13}C (see Experimental Section), ^2H-derived S^2_{axis} parameters were extracted with slightly higher precision because of the dominance of $J(0)$. It follows that the dynamics parameters considered most valuable (and the available field strengths) will often dictate whether ^2H or ^{13}C is more suitable. Another consideration for larger proteins (>10 kD) is spectral resolution in the $^1H/^{13}C$ correlation spectrum. The resolution in the ^2H experiments is limited due to the constant-time evolution period, and in addition the two- and three-bond ^2H isotope effects distort all methyl cross-peaks, which may make quantitation of volumes or intensities problematic. In the case of ^{13}C, the cross-peaks have no such distortions, and the resolution is limited by ^{13}C line widths. Because ^{13}C methyl line widths are narrow due to fast symmetry axis rotations, extremely high-resolution nonconstant-time spectra can be acquired for methyl regions of proteins. Finally, because the ^2H approach accesses the spectral density at the zero frequency, this approach may be favorable if complex motions of the symmetry axis exist, or if only one or two field strengths are available. If possible, data should be collected at two fields or more since the fitted parameters can then be meaningfully evaluated by a χ-squared statistic.

If the view of methyl dynamics provided by ^2H and ^{13}C relaxation methods are consistent, a unified approach should be advantageous for an EMF analysis. The ^2H $T_{1\rho}$ data contains valuable $J(0)$ information, thus allowing S^2_{axis} to be extracted easily, and the ^{13}C data has good sensitivity to τ_f versus τ_{axis} discrimination. Unfortunately, because α is greater than 1 we approach this "linked" analysis with some reservations. Since the relationship between $S^2_{axis}(^2H)$ and $S^2_{axis}(^{13}C,EMF)$ has been established experimentally given the present data and also because the differences in methyl rotation rates for CH$_3$ and CH$_2$D isotopomers may be significant, the protocol would be to obtain S^2_{axis} from ^2H relaxation, correct it using the empirically determined $\alpha = 1.2$, and then use this as input to fit τ_f

(66) Neuhaus, D.; Williamson, M. P. *The Nuclear Overhauser Effect in Structural and Conformational Analysis*; VCH Publishers: New York, 1989.

(67) Akke, M.; Palmer, A. G. *J. Am. Chem. Soc.* **1996**, *118*, 911-912.

(68) Ericsson, A.; Kowalewski, J.; Liljefors, T.; Stilbs, P. *J. Magn. Reson.* **1980**, *38*, 9-22.

(69) Hattori, A.; Crespi, H. L.; Katz, J. J. *Biochemistry* **1965**, *4*, 1213-1225.

(70) Hattori, A.; Crespi, H. L.; Katz, J. J. *Biochemistry* **1965**, *4*, 1225-1238.

(71) Makhatadze, G. I.; Clore, G. M.; Gronenborn, A. M. *Nat. Struct. Biol.* **1995**, *2*, 852-855.

(72) Jones, W. C.; Rothgeb, T. M.; Gurd, F. R. N. *J. Biol. Chem.* **1976**, *251*, 7452-7460.

(73) Piotto, M.; Saudek, V.; Sklenar, V *J. Biomol. NMR* **1992**, *2*, 661-665.

and τ_{axis} using the ^{13}C data at 500 and 600 MHz. This approach should be most useful if only a narrow range of field strengths are available.

Conclusions

From a comparative study of methyl dynamics in ubiquitin, ^2H and ^{13}C NMR spin relaxation approaches were found to yield the same principal features of ps−ns side-chain dynamics. It has become clear, however, that the two approaches offer complementary information on the details of the motions underlying relaxation. The ^2H approach has emerged as an efficient method for characterizing the degree of spatial restriction of the methyl symmetry axis. While the ^{13}C approach arrives at this order parameter with lower efficiency, the broad frequency distribution associated with ^{13}C relaxation made possible the discrimination between fast methyl rotation and symmetry axis reorientation. Finally, it was confirmed that the extended model-free form of the spectral density function currently provides the simplest, most realistic description of methyl dynamics in ubiquitin.

Supporting Information Available: Complete tables of ^2H and ^{13}C relaxation parameters (PDF). This material is available free of charge via the Internet at http://pubs.acs.org.

JA983758F